Original Paper

Molten Metal Flux Growth and Study of Properties and Chemical State of a New Compound $PrRh_{4.8}B_2$

Toetsu SHISHIDO[1,*], Masaoki OKU[1], Shigeru OKADA[2], Naoyuki NOGI[3], Tadaaki AMANO[4], Jinhua YE[5], Takao MORI[5], Masahiko TANAKA[5], Kiyoshi SHIMAMURA[5], Akira YOSHIKAWA[6], Ryoji SAHARA[1], Kunio YUBUTA[1], Vijay KUMAR[1], Akiko NOMURA[1], Takamasa SUGAWARA[1], Shin-ichiro TOZAWA[1], Kazuo OBARA[1], Naofumi OHTSU[1], Koichi HAYASHI[1], Kozo FUJIWARA[1], Noritaka USAMI[1], Shigemi KOHIKI[7], Katsuya TESHIMA[8], Shuji OISHI[8], Yoshiyuki KAWAZOE[1], Kazuo NAKAJIMA[1]

[1]Institute for Materials Research, Tohoku University, 2-1-1 Katahira, Aoba-ku, Sendai 980-8577
[2]Faculty of Science and Engineering, Kokushikan University, 4-28-1 Setagaya, Setagaya-ku, Tokyo 154-8515
[3]School of Engineering, The University of Tokyo, 7-3-1 Hongo, Bunkyo-ku, Tokyo 113-8656
[4]Shonan Institute of Technology, 1-1-25 Nishikaigan, Tujido, Fujisawa, Kanagawa 251-8511
[5]National Institute for Materials Science, 1-1 Namiki, Tsukuba 305-0044
[6]Institute of Multidisciplinary Research for Advanced Materials, Tohoku University, 2-1-1 Katahira, Aoba-ku, Sendai 980-8577
[7]Faculty of Engineering, Kyushu Institute of Technology, 1-1 Sensui-cho, Tobata-ku, Kitakyushu 804-8550
[8]Faculty of Engineering, Shinshu University, 4-17-1 Wakasato, Nagano 380-8553

Received October 11, 2007; E-mail: shishido@imr.tohoku.ac.jp

The hexagonal plate-like single crystals of a new compound $PrRh_{4.8}B_2$ were obtained by a molten metal flux growth method using Cu as a flux. $PrRh_{4.8}B_2$ is orthorhombic with the space group *Fmmm*; a = 0.9697(4), b = 0.5577(2) and c = 2.564(3) nm. The structure of the compound is of a modified $CeCo_3B_2$-type which is explained by a stacking model of Pr-B and rhodium layers. The temperature dependence of inverse static magnetic susceptibility, χ^{-1} obeys the Curie-Weiss law at temperatures above 50 K. The μ_{eff} is 4.2 μ_B and Θ_p is –13 K. The susceptibility deviates from the Curie-Weiss law below 50 K, suggesting some magnetic ordering. The value of micro-Vickers hardness for *c*-plane with the orthorhombic symmetry of $PrRh_{4.8}B_2$ is 6.7±0.6 GPa. The TG curve shows that oxidation of the $PrRh_{4.8}B_2$ proceeds above 873 K. Weight gain of the specimen heated up to 1473 K in air is 13 %. After TG-DTA measurement, final product is $PrBO_3$ and Rh. The X-ray photoelectron spectroscopic study and electron probe micro-analysis results show that a few monolayers of Cu atoms exist between the crystals of $PrRh_{4.8}B_2$.

Key Words: *$PrRh_{4.8}B_2$*, *Flux Growth*, *Crystal Structure*, *Magnetic Property*, *Hardness*, *TG-DTA*, *X-ray Photoelectron Spectrum*

1. Introduction

The crystal chemistry of R-Rh-B (R = rare earth element) systems has received considerable attention from many researchers in the fields of crystallography, magnetism, superconductivity, heavy-electron behaviour, valence fluctuations and catalytic properties[1-8]. The earlier paper provided the existence of six binary compounds, Pr_3Rh, Pr_7Rh_3, Pr_5Rh_3, Pr_5Rh_4, $PrRh_2$, and $PrRh_3$ for the Pr-Rh system[9]. Moreover, three compounds, Pr_2B_5, PrB_4 and PrB_6[10], and two compounds, Rh_7B_3 and RhB[11,12] were reported for Pr-B and for Rh-B systems, respectively. On the other hand, only two compounds, $PrRh_3B$[13] and $PrRh_3B_2$[14] were reported in the ternary Pr-Rh-B system. In this paper we report on the title compound, $PrRh_{4.8}B_2$ which is newly obtained by the molten metal flux growth method using Cu as flux. Growth, crystallographic data, magnetic properties, hardness, oxidation resistivity, and chemical state of the compound are presented.

2. Experimental details

2.1 Crystal growth

The starting materials used were small pieces of 99.9 % Pr, 99.9 % Rh powder and 99.9 % B powder. They were weighed in several atomic ratios of Pr, Rh and B, and mixed with 99.999 % of Cu powder in a weight ratio 1:10 for (Pr+Rh+B):Cu. The mixture of the four elements was placed in a high purity (99.9 %) dense alumina crucible, which was inserted in a vertical electric furnace. Ar was flowing at a rate of 200 mL·min^{-1} in the furnace as a protecting atmosphere against oxidation. Then the mixture of the starting materials was heated at a rate of 673 K·h^{-1} up to 1673 K, and kept at that temperature for 10 h, and then slowly cooled down at a rate of 10 K·h^{-1} to 1353 K. Temperature was controlled at the bottom of the crucible during all heating and cooling processes. At 1673 K, the soaking temperature of the solution, the height of the melt was about 30 mm and the temperature at the melt surface and the bottom was 1643 K and 1673 K, respectively. After the temperature reached 1353 K, the furnace was rapidly cooled down to room temperature. The grown crystals were separated by dissolving Cu in diluted nitric acid.

2.2 Characterization

The surface of the crystals was analyzed by scanning electron microscope (SEM). The chemical analysis was carried out using the inductively coupled plasma (ICP) technique after fusion of the samples with NH_4HSO_4. The X-ray analyses were performed using a Burger precision camera with zirconium-filtered Mo*Kα* radiation and a four-circle X-ray diffractometer with graphite-monochromatized Mo*Kα* radiation. The magnetic properties were determined with a pendulum-type magnetometer in the temperature range of 1.8 to 300 K. Micro-Vickers hardness (MVH) of the as-

grown single crystals was measured at room temperature. A load of 100 g was applied for 15 s and ten impressions were recorded for each individual face of the crystal. The obtained values were averaged and the experimental error was estimated. Thermo-gravimetric (TG) analysis and differential thermal analysis (DTA) were performed between room temperature and 1473 K to study the oxidation resistivity of the crystals in air. A sample of about 25 mg was heated at a rate of 10 $K \cdot min^{-1}$ up to 1473 K. The oxidation products were analyzed by powder X-ray diffractometry. Initial oxidation behavior of the specimen was examined by X-ray photoelectron spectroscopy (XPS). The XPS spectra were taken from the following two conditions: (i) clean surfaces coated with no oxide layer prepared by fracturing the specimen in an ultra high vacuum and (ii) surface oxidized by exposing the fractured surface to high purity oxygen at a pressure of 1.3×10^{-6} Pa.

3. Results and Discussion

3.1 Morphology and crystal structure of the single crystals

Single crystals in the form of a hexagonal plate and powder like crystals were extracted at the starting composition Pr:Rh:B = 1:3:1. In this paper, we focus our attention on the hexagonal plate-like single crystals. They have silver metallic luster and the mean size of the crystals is approximately 5 mm (width) × 0.5 mm (thickness). The chemical analysis of the plate-like crystals indicates that the chemical formula of the compound is $PrRh_{4.8}B_2$. Figure 1(a) shows a SEM image of a hexagonal plate-like single crystal. Figure 1(b) is an enlargement of the corresponding region indicated by an arrow in (a) and it reveals the terrace growth. The phase diagram of the Pr-Rh-B system is shown in Fig.2. Six binary intermetallic compounds, Pr_3Rh, Pr_7Rh_3, Pr_5Rh_3, Pr_5Rh_4, $PrRh_2$, and $PrRh_3$ exist in the Pr-Rh system. Three compounds, Pr_2B_5, PrB_4, and PrB_6 also exist in the Pr-B system while Rh-B system involves two compounds, Rh_7B_3 and RhB. The authors have reported the formation of $PrRh_3B$ in the Pr-Rh-B ternary system[13]. This compound is perovskite-type boride and it has cubic symmetry (space group; $Pm\bar{3}m$). Ternary boride $PrRh_3B_2$ has been reported by Ku *et al.*[14]. It has a hexagonal $CeCo_3B_2$-type structure which can be derived from the $CaCu_5$-type structure with the *P6/mmm* space group. The compositional position of a new compound $PrRh_{4.8}B_2$ is shown in Fig.2. As a result, $PrRh_3B$, $PrRh_3B_2$ and a new compound $PrRh_{4.8}B_2$ exist in the rhodium-rich portions of the Pr-Rh-B ternary phase diagram.

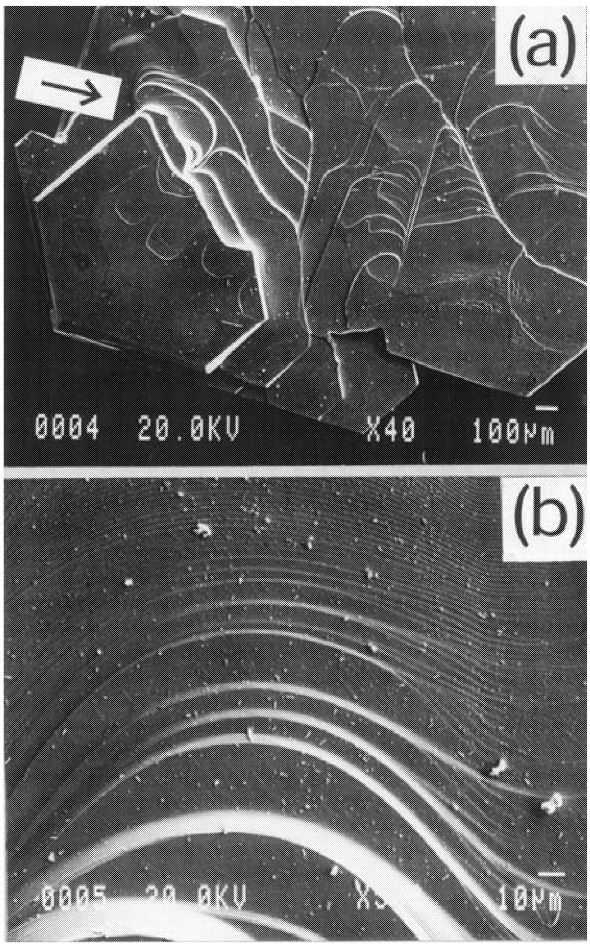

Fig.1 SEM image of a hexagonal plate-like single crystal of $PrRh_{4.8}B_2$.

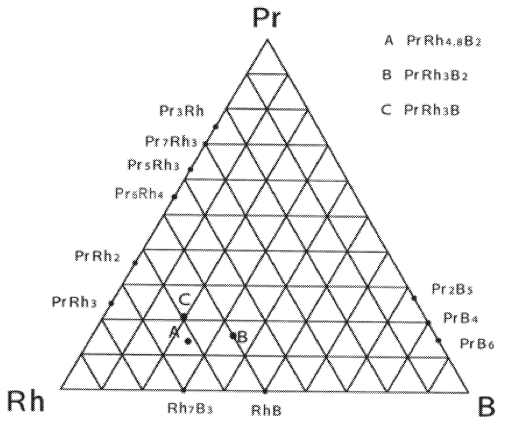

Fig.2 Compositional position of the new compound $PrRh_{4.8}B_2$ on the phase diagram of Pr-Rh-B. Previously reported compounds $PrRh_3B$ and $PrRh_3B_2$ are also shown in the figure.

The X-ray structure analysis of the single crystal reveals that the compound is orthorhombic with a space group *Fmmm* and the lattice parameters are a = 0.9697(4), b = 0.5577(2), and c = 2.564(3) nm, respectively[8]. The basic crystal data are presented in Table 1. The arrangement of the atoms in the crystal is shown in Fig. 3 with (a) showing the perspective drawing of the full structure

Table 1 Crystallographic data of $PrRh_{4.8}B_2$.

Chemical formula	$PrRh_{4.8}B_2$[a]
Crystal system	Orthorhombic
Structure type	Modified-$CeCo_3B_2$
Space group	*Fmmm*
Lattice parameter (nm)	
a	0.9697(4)
b	0.5577(2)
c	2.564(3)
Formula units per unit cell	12

[a]Formula unit determined by the chemical and structural analyses.

of $PrRh_{4.8}B_2$ and (b), the Kagome (3636) nets of rhodium atoms (z = ±0.2) as seen along the c-axis. The structure of this compound is a modified $CeCo_3B_2$-type and it is made up of $PrRh_3B_2$-block and 'partly-occupied Rh layer', parallel to the (001) plane. The $PrRh_3B_2$-block consists of two different infinite layers: one of them is a Pr-B layer and the other, a Rh layer. The chemical formula of this compound as obtained from X-ray analysis is $PrRh_{4.8}B_2$ and it is in agreement with the chemical analysis described above.

3.2 Magnetic properties

The temperature dependence of the inverse static magnetic susceptibility, χ^{-1} and the magnetization curves at 4.7 K and room temperature are shown in Fig.4 and Fig.5, respectively. The inverse susceptibility deviates from the Curie-Weiss law below 50 K and the magnetization curve at 4.7 K has a small weak ferromagnetic component, suggesting some magnetic ordering. In all the cases the magnetic field is applied in the thin c-plane. The effective magnetic moment of the Pr ion and the Curie-Weiss temperature were determined from the slope and the intercept of the straight line with the T-axis, respectively. The μ_{eff} is 4.2 μ_B and Θ_P is –13 K. The value of the effective magnetic moment is larger than the theoretical Hund's value of 3.6 μ_B for the free trivalent ion Pr^{3+}.

3.3 Hardness [15]

As presented in Table 2, the value of MVH for c-plane of the orthorhombic symmetry of $PrRh_{4.8}B_2$ is 6.7 ± 0.6 GPa. The data for $PrRh_3B$, $PrRh_3B_2$, Rh_3B and Rh_7B_3 are also listed in the table. Samsonov and Vinitskii pointed out that the hardness of the binary borides increases with boron content in the system of Rh and B[15,16]. This tendency of the binary borides is also found in the ternary borides that are composed of Pr, Rh and B elements. Considering the lower boron content in ternaries, the hardness of $PrRh_3B_2$ is relatively high. This result suggests that the hardness of the boride depends on not only boron content in the compound but also on other factors, for example, the crystal structure of each compound.

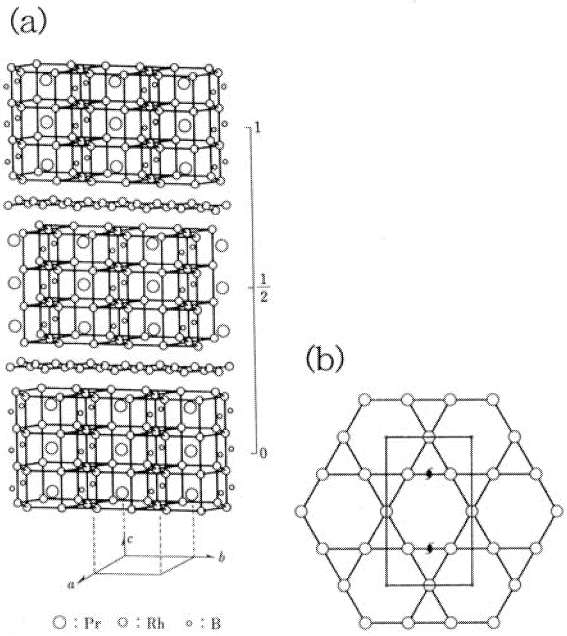

Fig.3 (a) Perspective drawing of the full structure of $PrRh_{4.8}B_2$ and (b) the Kagome (3636) nets of rhodium atoms (z = ± 0.2) as seen along the c-axis[8].

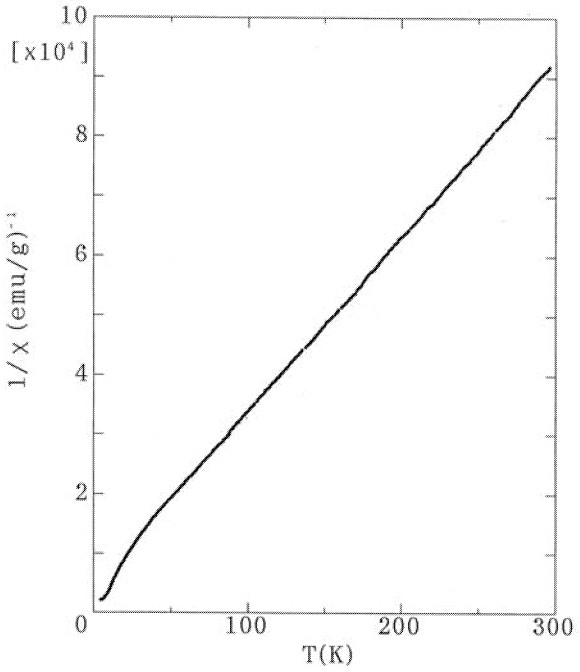

Fig.4 The temperature dependence of the inverse static magnetic susceptibility, χ^{-1} of $PrRh_{4.8}B_2$.

3.4 TG-DTA

The TG-DTA curves for $PrRh_{4.8}B_2$ in air are shown in Fig.6 as solid lines. The data for $PrRh_3B$ and $PrRh_3B_2$ measured under the same conditions are also shown in the figure as references. The TG curve shows that the oxidation of $PrRh_{4.8}B_2$ proceeds above 873 K. Above 1273 K weight loss may correspond to the evaporation of boron oxide. Weight gain of the specimen heated up to 1473 K in

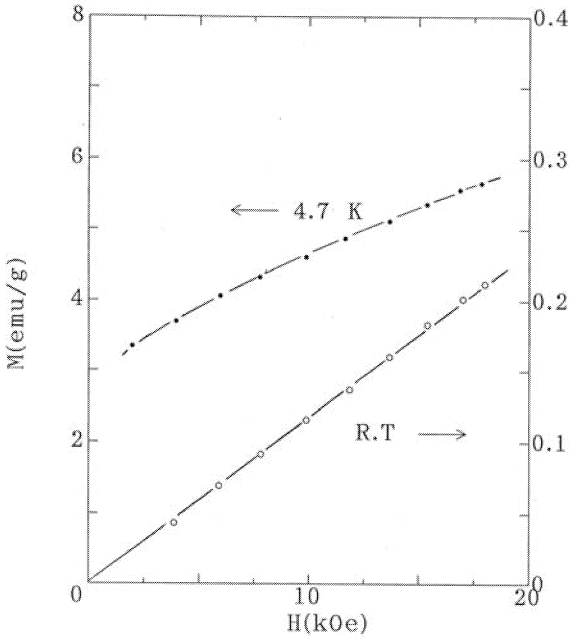

Fig.5 The magnetization curves at 4.7 K and room temperature.

Table 2 Vickers microhardness of the $PrRh_{4.8}B_2$ and related compounds that exist in the Pr-Rh-B ternary system.

Compound	Boron content (atom%)	Crystal structure	Microhardness (Hv, GPa)	References
$PrRh_{4.8}B_2^a$	25.6	Orthorhombic	6.7 ± 0.6	This study
$PrRh_3B^b$	20.0	Cubic	8.2 ± 0.1	[15]
$PrRh_3B_2^b$	33.3	Hexagonal	10.5 ± 0.3	[15]
RhB^c	50.0	Hexagonal	12.13	[16]
$Rh_7B_3^c$	30.0	Hexagonal	7.77	[16]

Values for the compounds belonging to Rh-B binary system are also given.
[a]Single crystal.
[b]Polycrystal.
[c]Not shown single crystal or polycrystal.

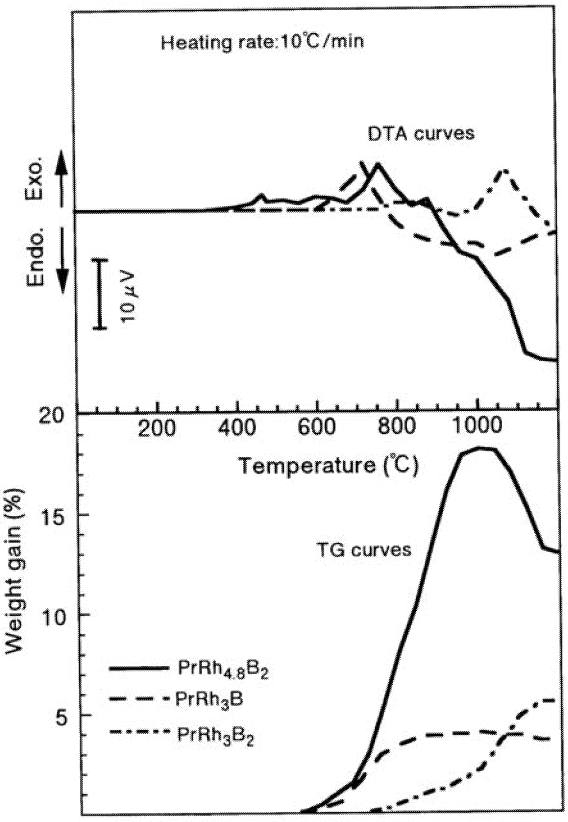

Fig.6 TG-DTA curves (solid lines) for $PrRh_{4.8}B_2$. Data for $PrRh_3B$ and $PrRh_3B_2$ are presented as references.

air is 13 %. In the DTA curve, the exothermic peaks caused by oxidation are found at 753 K, 1033 K and 1153 K, respectively. Above 1173 K, DTA curve largely deviates from straight line to endothermic site. This phenomenon is ascribable to the evaporation of boron oxide. The final products, obtained by heating up to 1473 K, were $PrBO_3$ (orthorhombic symmetry) and Rh (cubic symmetry). Phenomenal temperature and weight gain from TG-DTA measurement for $PrRh_{4.8}B_2$ are summarized in Table 3.

Basically, resistance to oxidation of a compound relates to its crystal structure[6]. As mentioned above, the structure of $PrRh_{4.8}B_2$ can be described by sheets of modified $CeCo_3B_2$-type structure stacked along the *c*-direction. $PrRh_{4.8}B_2$ single crystals display

Table 3 Phenomenal temperature, weight gain and final product from the TG-DTA measurement in air for $PrRh_{4.8}B_2$.

Sample	Oxidation proceeded by TGA (℃)	Exothermal maximum by DTA (℃)	Weight gain by TGA (%)	Final products
$PrRh_{4.8}B_2$	> 600	480, 760, 880	13	$PrBO_3$ and Rh

extremely plastic character and they are easy to cleave parallel to the (001) plane. This fact suggests that the weak bonding occurs between the sheets through the 'partly-occupied rhodium sheets'. It is well known that the layer structure compounds, for example, $CaZn_5$-type[17-21] and Th_2Ni_{17}-type[22], exhibit high affinity for H_2, N_2, etc. Poor oxidation resistance of $PrRh_{4.8}B_2$ can be explained by its characteristic layer structure, especially the existence of 'partly-occupied rhodium sheets'. On the other hand, reference sample of $PrRh_3B$ represents high oxidation resistance (Fig.6). Crystal structure of $PrRh_3B$ is cubic (space group; $Pm\bar{3}m$)[13] and therefore it behaves as isotropic with regard to oxidation and it shows high resistance to oxidation. $PrRh_3B_2$ has hexagonal symmetry with $CeCo_3B_2$-type (space group; *P6/mmm*) structure[14] and its resistance to oxidation is medium among the three ternary borides (Fig. 6). As a result, the oxidation resistivity of $PrRh_{4.8}B_2$ is low. However, the authors have a strong interest in the affinity of this compound for H_2 from the viewpoint of hydride-forming intermetallic compounds, because this compound is one of the variations of the $CaZn_5$-type structure. The determination of the H_2 sorption in $PrRh_{4.8}B_2$ is currently under way.

3.5 Chemical state

SEM images taken from EPMA of the fractured surface and Pr$L\alpha$, Rh$L\alpha$, Cu$K\alpha$ X-ray images are shown in Fig.7. It is found that Pr and Rh are uniformly distributed throughout the specimen, but that Cu is in-homogeneously distributed. Because measurements are carried out with a spot size of 300 μmφ in the XPS analysis, the images represent two-dimensionally averaged composition. Figure 8 shows XPS survey spectrum for the fractured $PrRh_{4.8}B_2$ surface. XPS survey spectrum for the surface layers yields photoelectron peaks belonging to nominal elements of Pr, Rh and B. Furthermore, Cu Auger peaks are observed at *ca.* 570 eV, indicating that Pr 3d and Cu 2p peaks are overlapping. It was difficult to estimate the relative concentrations of the elements due to the overlap of the major photoelectron peaks. Initial oxidation behavior of the specimen was examined by the comparison of the as-fractured spectrum with the oxidized spectrum, as shown in Fig.9, Fig.10, and Fig.11. In the Pr 3d and Cu 2p regions for the as-fractured specimens, two peaks corresponding to spin-orbit splitting are observed (Fig.9(a)). The binding energy for the lower energy peak is 932.0 eV which is 0.2 eV higher than that of Pr $3d_{5/2}$ peak for elemental Pr and 0.7 eV lower than that of Cu $2p_{3/2}$ for elemental Cu[23]. The result would be due to the overlap between Pr 3d and Cu 2p peaks. After exposing to low-pressure oxygen atmosphere, two new peaks appear at 932.9 eV and 929.0 eV (Fig.9(b)). These peaks correspond to those of Pr_2O_3 and satellite peak associated with Pr_2O_3, respectively[24], indicating that one of the initial oxides formed on $PrRh_{4.8}B_2$ is Pr_2O_3. In the spectrum as shown in Fig.10, in Rh region no significant difference is observed between the as-fractured and the oxygen-exposed surfaces, indicating that Rh is not oxidized in the low-pressure oxygen atmosphere. The binding energy of B 1s peak for the as-fractured surface is 188.3 eV (Fig. 11(a)), which is lower than that of elemental B[23]. This trend is similar to the $HoRh_3B$ case[25]. After the exposure to oxygen, new peak appears at 191.7 eV (Fig.11(b)), the value of which agrees with boron-oxide. Similar to

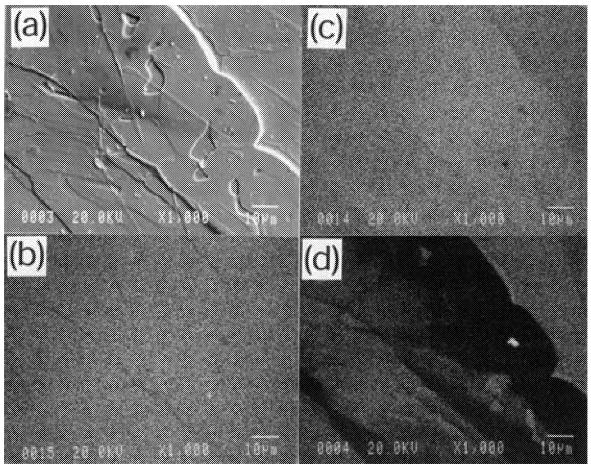

Fig.7 (a) SEM image of the fractured surface of the crystal. (b) Pr*L*α, (c) Rh*L*α, and (d) Cu*K*α X-ray images are also shown.

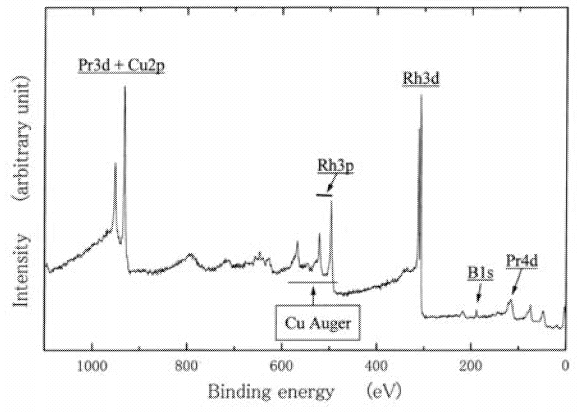

Fig.8 Wide range XPS spectrum of $PrRh_{4.8}B_2$ fractured in the spectrometer.

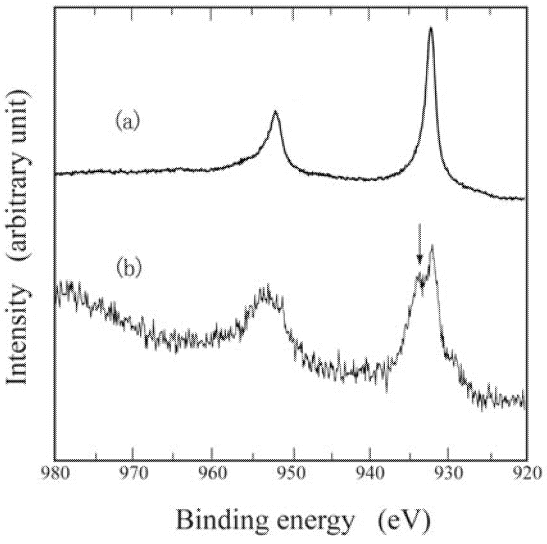

Fig.9 Pr 3d and Cu 2p XPS spectra for the two states of the sample, (a) fractured in the spectrometer and (b) exposed to oxygen for 300 s after (a).

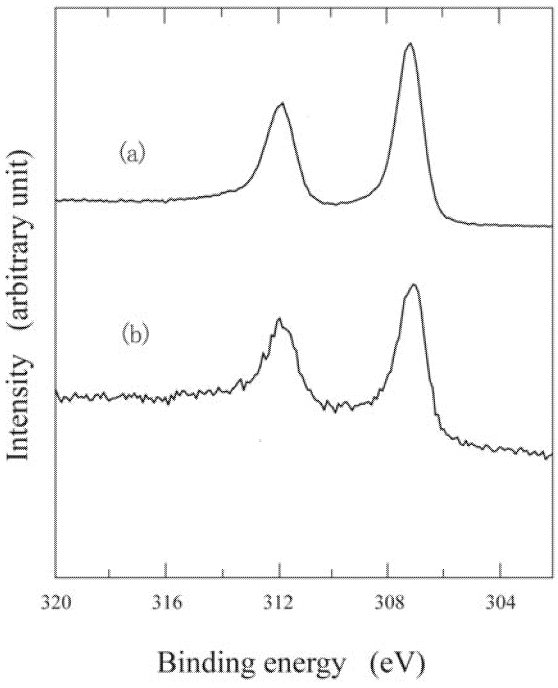

Fig.10 Rh 3d XPS spectra for the two states of the sample, (a) fractured in the spectrometer and (b) exposed to oxygen for 300 s after (a).

the initial oxidation behavior of hafnium hydride[26], the oxidation of Pr and B on $PrRh_{4.8}B_2$ proceeded very rapidly, whereas the oxide of Rh is not observed after the oxygen-exposure. The result indicates that oxidations of Pr and B occurred prior to that of Rh.

Even in case where the specimen was fractured in air, B 1s peak which is ascribed to the compounds was observed. This means that kinetic energy of B 1s photoelectron is larger than that of Pr 3d and that B 1s spectra have more profound information from deeper layer than B 3d spectra do. According to EPMA, ratio of Cu/Pr in the specimen is in the range of 0.20 and 1.53[8]. However, in the analysis of crystal structure by means of XRD, the reliability factor for the case where Cu is assumed to be involved in the specimen is worse than that for the case where Cu is assumed to be absent and also no peak was observed in XRD at all. From these facts and also from the change of XPS spectrum, it can be concluded that Cu atoms exist sporadically between the crystals of $PrRh_{4.8}B_2$, forming domains as thick as a few atomic layers.

4. Conclusions

The authors can draw the following conclusions from this study.

(1) A new compound $PrRh_{4.8}B_2$ with silver metallic luster is successfully grown in the form of hexagonal plates (~ 5 × 0.5 × 0.5 mm^3) by solution growth method using Cu as flux. Cu acted as a good intermediate[27-30] for the crystal growth of this new ternary boride.

(2) $PrRh_{4.8}B_2$ belongs to an orthorhombic system with the space group *Fmmm*. The lattice parameters are a = 0.9697(4), b = 0.5577(2) and c = 2.564(3) nm, respectively. The structure of the compound is a modified $CeCo_3B_2$ type which is explained by a stacking model of Pr-B and rhodium layers.

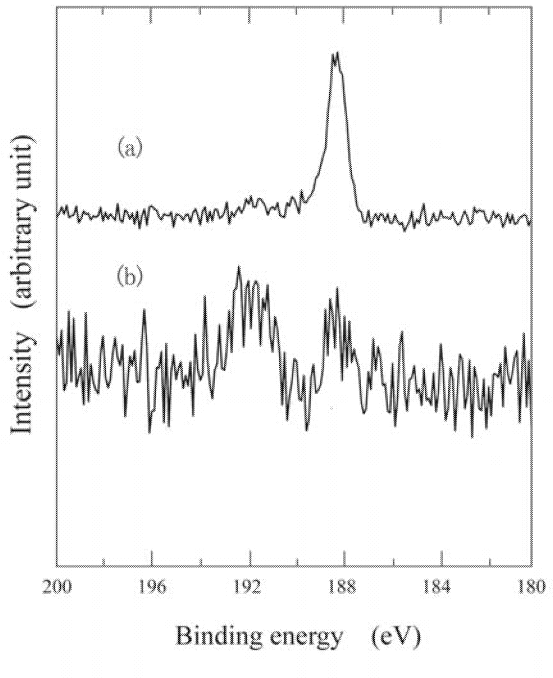

Fig.11 B 1s XPS spectra for the two states of the sample, (a) fractured in the spectrometer and (b) exposed to oxygen for 300 s after (a).

(3) The temperature dependence of inverse static magnetic susceptibility, χ^{-1} obeys the Curie-Weiss law at higher temperature above 50 K. The μ_{eff} is 4.2 μ_B (Hund's value for Pr^{3+}: 3.6 μ_B) and Θ_p is –13 K. The susceptibility deviates from the Curie-Weiss law, below 50 K, suggesting some magnetic ordering.

(4) The value of MVH for *c*-plane with the orthorhombic symmetry of $PrRh_{4.8}B_2$ is 6.7 ± 0.6 GPa.

(5) The TG curve represents that oxidation of $PrRh_{4.8}B_2$ proceeds above 873 K. Weight gain of the specimen heated up to 1473 K in air is 13 %. After oxidation measurement, final product is $PrBO_3$ (orthorhombic symmetry) and Rh (cubic symmetry).

(6) The X-ray photoelectron spectroscopic study and electron probe micro-analysis results show that a few monolayers of Cu atoms exist between the crystals of $PrRh_{4.8}B_2$.

Acknowledgements

This study was partly supported by a Grant-in-Aid for Science Research from the Ministry of Education, Science and Culture of Japan, and was performed under the cooperative research program of ARCMG in IMR, Tohoku University. We are grateful to Prof. I. Higashi of Chiba Institute of Technology for his valuable discussions. VK thankfully acknowledges the kind hospitality at the International Frontier Center for Advanced Materials of IMR.

References

1) M. P. B. Maple, O. Fischer (Eds.), *Superconductivity in Ternary Compounds*, *Topics in Current Physics*, *vol.34*, Springer, Berlin, **1982**.
2) T. Shishido, T. Fukuda, *J. Chem. Ind. Chem. the Chem. Soc. Jpn.*, **1993**, *5*, 677.
3) J. Bernhard, I. Higashi, P. Granberg, L. E. Tergenius, T. Lundström, T. Shishido, A. Lukolainen, H. Takei, T. Fukuda, *J. Alloys Compd.*, **1993**, *193*, 295.
4) T. Shishido, I. Higashi, H. Kitazawa, J. Bernhard, H. Takei, T. Fukuda, *Jpn. J. Appl. Phys. Ser.*, **1994**, *10*, 142.
5) J. Bernhard, *Jpn. J. Appl. Phys. Ser.*, **1994**, *10*, 148.
6) T. Shishido, J. Ye, M. Oku, K. Kudou, T. Sasaki, T. Matsumoto, T. Fukuda, *J. Alloys Compd.*, **1997**, *248*, 18.
7) T. Shishido, J. Ye, T. Sasaki, R. Note, K. Obara, T. Takahashi, T. Matsumoto, T. Fukuda, *J. Solid State Chem.*, **1997**, *133*, 92.
8) I. Higashi, T. Shishido, F. Takei, T. Kobayashi, *J. Less-Common Metals*, **1988**, *39*, 211.
9) Z. Blazina, R. C. Mohanty, A. Raman, *Z. Metallkunde*, **1987**, *78*, 485.
10) K. E. Spear, in: A. M. Alper (Ed.), *Phase Diagrams: Materials Science and Technology*, *vol.6*, Academic Press, New York, **1976**, p.91.
11) V. A. Kosenko, B. M. Rud, V. G. Sidorova, *Russian Inorganic Materials*, *vol.7*, *English trans.*, Plenum Press, New York, **1970**, p.1294.
12) G. Reinacher, *Rev. Metall.*, **1957**, *54*, 321.
13) H. Takei, T. Shishido, *J. Less-Common Met.*, **1984**, *97*, 223.
14) H. C. Ku, G. P. Meisner, F. Acker, D. C. Johnston, *Solid State Commun.*, **1980**, *35*, 91.
15) G. V. Samsonov, I. M. Vinitskii, *Handbook of Refractory Compounds*, IFI/Plenum, New York, **1980**, p. 303.
16) S. Okada, K. Kudou, T. Shishido, Y. Sato, T. Fukuda, *J. Ceram. Soc. Jpn.*, **1999**, *2*, 184.
17) K. H. J. Buschow, H. H. Van-Mal, A. R. Miedema, *J. Less-Common Met.*, **1975**, *42*, 163.
18) O. Boser, *J. Less-Common Met.*, **1976**, *46*, 91.
19) W. E. Winsche, K. C. Hoffman, F. J. Salzanc, *Science*, **1973**, *180*, 1325.
20) J. H. N. Van Vucht, F. A. Kujipers, H. C. A. M. Bruning, *Philips Res. Rep.*, **1970**, *25*, 133.
21) H. Sun, T. Tomida, K. Makita, Y. Maehara, *J. Alloys Compd.*, **1996**, *237*, 108.
22) S. Yajima, H. Kayano, *J. Less-Common Met.*, **1977**, *55*, 139.
23) C. D. Wagner, W. M. Riggis, L. E. Davis, J. F. Moulder, *Hand Book of X-ray Photoelectron Spectroscopy*, ed. by G. E. Muilenberg, Perkin-Elmar Co., Minesota, **1978**.
24) H. Ogasawara, A. Kotani, R. Potze, G. A. Sawatzky, B. T. Thole, *Phys. Rev.*, **1991**, *B44*, 5465.
25) T. Shishido, M. Oku, T. Sasaki, H. Iwasaki, H. Kishi, H. Horiuchi, T. Fukuda, *J. Alloys Comd.*, **1995**, *283*, 91.
26) N. Ohtsu, B. Tsuchiya, M. Oku, T. Shikama, K. Wagatsuma, *Appl. Surf. Sci.*, **2007**, *253*, 6844.
27) J. Ye, T. Shishido, T. Fukuda, K. Nakajima, *J. Cryst. Growth*, **2001**, *229*, 521.
28) T. Shishido, S. Okada, J. Ye, A. Nomura, J. Ye, K. Nakajima, *Crystal Letters*, **2006**, 163.
29) T. Shishido, S. Okada, J. Ye, M. Tanaka, T. Mori, K. Kudou, K. Iizumi, Y. Sawada, K. Teshima, S. Oishi, N. Nogi, A. Nomura, T. Sugawara, H. Kojima, R. Sahara, K. Yubuta, K. Hayashi, M. Oku, Y. Kawazoe, K. Nakajima, *J. Flux Growth*, **2006**, *1*, 47 [in Japanese].
30) T. Shishido, S. Okada, J. Ye, A. Nomura, K. Nakajima, *J. Flux Growth*, **2007**, *2*, 14 [in Japanese].